Nonlinear absorption properties correlated with the surface and structural changes of ultra short pulse laser irradiated CR-39

**M. Shahid Rafique · Shazia Bashir · Ali Ajami ·
Wolfgang Husinsky**

Abstract We have investigated femtosecond laser irradiation effects on the surface topography, structural changes and nonlinear absorption properties of CR-39. For this purpose, a CR-39 target was exposed in air to 25 fs, 800 nm Ti: sapphire laser radiation at fluences ranging from $0.25\,\mathrm{J\,cm^{-2}}$ to $3.6\,\mathrm{J\,cm^{-2}}$. The surface of irradiated CR-39 probed by an Atomic Force Microscope (AFM) exhibits the formation of several topographical structures, like bumps, explosions and nano cavities. Raman spectroscopy is performed to explore chemical and structural modification of the irradiated target. The spectroscopy reveals changes such as cross linking, bond breaking, formation of new bonds etc. in the fundamental structure of the polymer after irradiation. In order to establish a correlation between morphological and structural changes with the changes in the nonlinear absorption of the irradiated CR-39, a Z-scan technique was employed. A comparison of experimentally obtained data from Z-scan measurements with our calculations predicts the dominance of three-photon absorption in the case of pristine CR-39, whereas for irradiated targets concurrence of three- and two-photon absorption is probable. Nonlinear absorption increases with increasing laser fluences and is well correlated by surface and structural changes revealed by AFM and Raman spectroscopy.

M.S. Rafique (✉) · S. Bashir · A. Ajami · W. Husinsky
Institute of Applied Physics, Technical University Vienna,
8-10 wiednerhaupstrasse, 1040, Vienna, Austria
e-mail: shahidrafiq@uet.edu.pk

M.S. Rafique
Physics Department, University of Engineering and Technology,
54890, Lahore, Pakistan

1 Introduction

The importance of polymers with improved surface and bulk properties has increased substantially due to their technological applications in microelectronics, packing industry and medicines [1]. Irradiation of polymers by neutrons [2], protons [3], slow and swift heavy ions [4], gamma rays [5], UV [6] and IR lasers [7–9] results in the modification of structural, optical, chemical and mechanical properties of the polymers. The effectiveness of these changes depends upon the basic structure of the polymer and the experimental conditions of exposure such as dose, energy and wavelength of incident radiation.

CR-39 is a polymer from diallyl monomers, particularly poly diethylene glycol-bis-allyl carbonate or allyl diglychol carbonate and is commercially known as CR-39 (Columbia Resin 39 or Allymer 39). Its chemical formula is
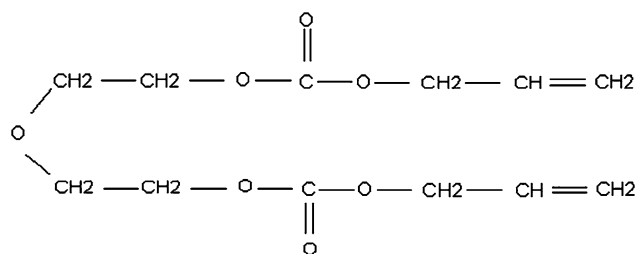
CR-39 is an important polymer, which is known as an excellent material for a number of industrial, medical and optical applications. It is extensively used in various experiments in fusion research, nuclear science and astrophysics [10, 11]. However, few studies have been performed to obtain fundamental information on the laser irradiation effects on this detector material [7, 8]. Most recent work on CR-39 reports that neutron, gamma and high-energy ion irradiation induces changes in its structural and optical properties [2, 4, 10–12].

Investigations on the nonlinear optical properties of composite [13] and pure CR-39 [14] have also been reported in the literature.

In the present work, the surface, structural and chemical changes induced by femtosecond laser irradiation on CR-39 has been explored. The object is to correlate these changes with the changes in the nonlinear absorption properties of this polymer after irradiation.

2 Experimental details

CR-39 is irradiated in air with laser pulses obtained from a multipass CPA Ti: sapphire amplifier seeded from a mode-locked Ti: Sapphire oscillator. The system operating at a repetition rate of 1 KHz provides laser pulses with a central wavelength around 800 nm and a typical pulse length of 25 fs. A CR-39 target (20 mm × 20 mm × 1 mm) was mounted on a *xyz*-manipulator with a spatial resolution of 5 μm in each direction for a precise positioning of the sample for each exposure. The laser beam, after passing through a 36 cm focal length lens, was incident perpendicular to the surface of the target placed 5 mm away from the focus point giving a spot size of 100 μm. The irradiation fluence was varied from 0.2 J cm^{-2} to 3.6 J cm^{-2}. In order to expose the target, a surface area of approximately 1 mm × 1 mm was irradiated by overlapping individual laser spots. The laser beam profile (intensity and shape) was monitored with a Laser Cam–HR (Coherent) to ensure that the beam shape was Gaussian. Investigations on the surface of the laser irradiated CR-39 were performed with a MFP-3D scanning force microscope (Asylum Research USA) in contact mode under ambient conditions.

The Raman spectroscopy is done using aLab Ram HR-800 (Horiba Jobin-Yvon) Raman spectrometer. A He–Ne laser is used as an excitation source with 8 mW power, at 632.8 nm.

The main aim of the measurements reported here was to correlate AFM surface topography and the Raman spectroscopy with the nonlinear absorption properties of irradiated CR-39. For this purpose, an open aperture Z-Scan technique [15] has been employed. This technique allows the nonlinear absorption coefficients (Two-photon Absorption (TPA) or Three-photon Absorption (ThPA)) of the material [14] to be determined. In this technique, the system delivers ultrashort laser pulses with a repetition rate of 1 kHZ. The pulse width estimated as the FWHM of a Gaussian temporal profile, is typically 25 fs and the spectrum is concentrated at 800 nm. The irradiated CR-39 targets were mounted on a translating stage that can be moved across 25 mm through the beam focus. The irradiated targets were scanned by the laser beam at a scanning energy of 100 nJ. The beam was focussed through a lens of focal length 20 cm with a beam waist of 14 μm and a Rayleigh length of 0.8 mm.

3 Results and discussion

3.1 AFM measurements

Figure 1 presents AFM topographic images (2 μm × 2 μm with different heights) of ultra short laser irradiated CR-39 at a fluence of 0.2 J cm^{-2} (a), 0.5 J cm^{-2} (b), 1.5 J cm^{-2} (c, d), 2.5 J cm^{-2} (e) and 3.6 J cm^{-2} (f). Localized nanostructures in the form of bumps are clearly seen on the irradiated surface. Heights and diameters of these bumps range from 5–20 nm and 100–300 nm, respectively. An increase in the diameter and number density of these bumps is observed with the increasing laser fluences from 0.2 J cm^{-2} to 2.5 J cm^{-2}. However, at a laser fluence of 1.5 J cm^{-2}, an additional feature in the form of explosions or nanocavities with diameter ranging from 50–100 nm and depths 1–5 nm at the top of the bumps are also observed (1d). If the laser fluence is increased up to 3.6 J cm^{-2}, it appears that there is an onset of material ejections which results in craters (2f). This fluence is assumed to be sufficiently high to cause explosive ablation.

Dependence of geometric characteristics (diameters and heights) and number of bumps on the laser fluence can be quantitatively evaluated from AFM images (Fig. 1(a–e)). Different sizes of protrusions can be explained on the basis of marked differences in the energy deposition and the material ejection mechanism. During an expansion of laser-induced vapor/plasma, the density of vapor phase species is significantly non-uniform due to the plasma composition and various processes involved such as absorption of laser radiation, ultrafast melting, ionization, recombination, condensation and clustering. It has been reported [16] that there is an irregular variation in the melting point of selected atomic clusters i.e. smaller particles have a lower melting point than bulk material. This irregular variation in melting point also causes size variation of the bumps. At the early stage, a single atom is sputtered. This single atom diffuses by interstitial paths where two atoms attract each other and form a stable dimer. This dimer can push further atoms off from their original lattice sites and occupy the vacancy. It has ability to attach another atom to form a trimer which causes lattice deformation. Consequently, there is occurrence of variation in the rate of nucleation and growth of clusters. This variation marks a significant difference in the sizes of bumps. These bumps are discrete localized aggregates of atoms (agglomerates), which cannot escape from the surface and are frozen in the form of protrusions or bumps.

The formation of these bumps and nano cavities can be explained on the basis of thermo elastically induced stresses caused by laser-induced heating within the material. These stresses stay confined in the focal volume leading to a maximum pressure rise [17]. This pressure may exceed the Young modulus of CR-39 and cause rupturing or phase explo-
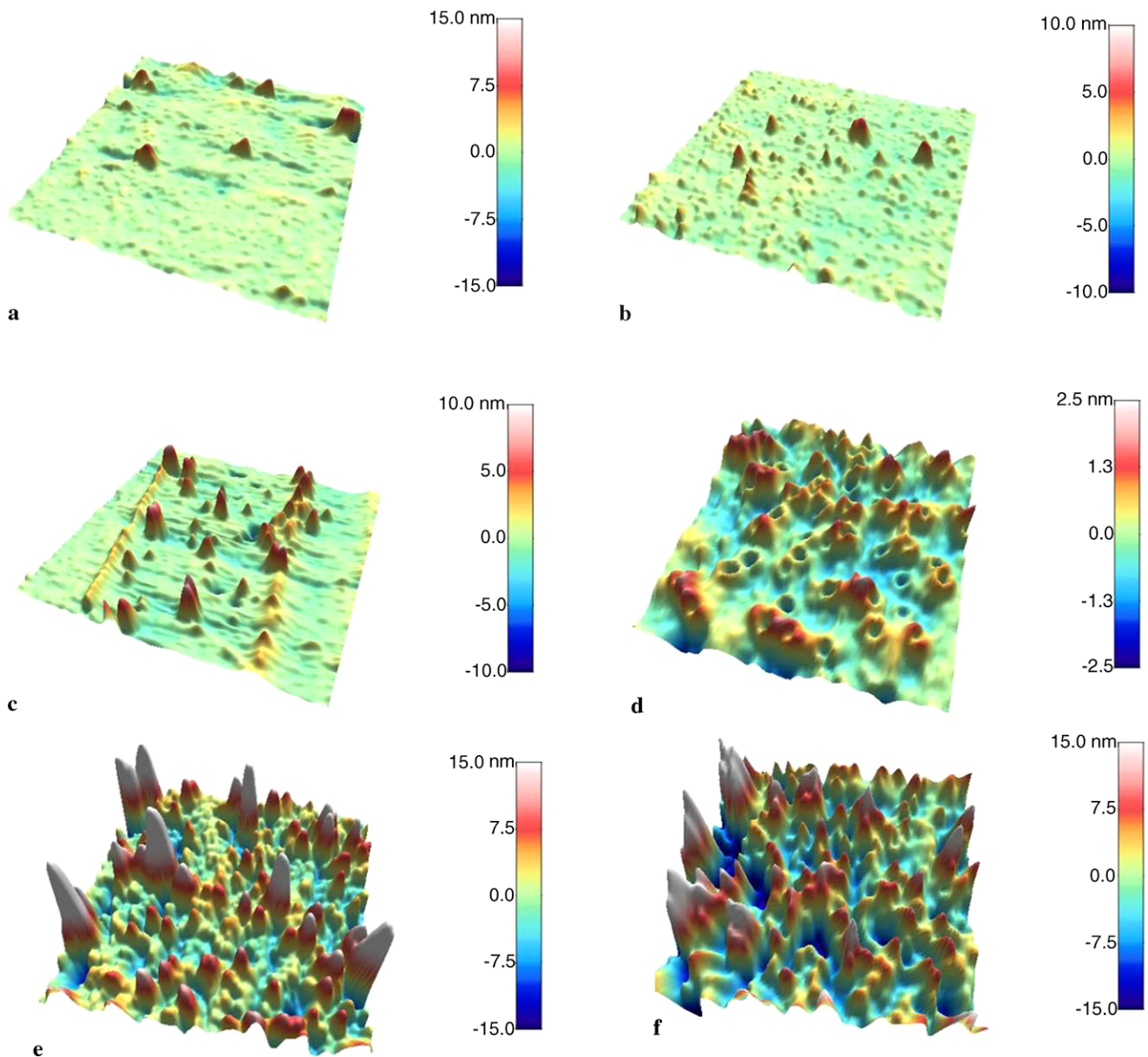
Fig. 1 AFM topographic images (2 μm × 2 μm with different heights) of femtosecond laser (800 nm, 25 fs) irradiated CR-39 at fluence (**a**) 0.25 J cm^{-2}, (**b**) 0.5 J cm^{-2}, (**c**) 1.5 J cm^{-2} (bumps are prominent), (**d**) 1.5 J cm^{-2} (nanocavities are prominent), (**e**) 2.5 J cm^{-2}, (**f**) and 3.6 J cm^{-2}

sion which is a possible physical reason for the melt ejection [18].

Another possible explanation for the bump formation could be that the plasma generation in the focal region increases the absorption coefficient and produces a fast energy release in a very a small volume. The total deposited energy builds up the pressure that drives the shock wave. This shock wave propagates into the surrounding cold material. After the release of pressure, the shock-affected material undergoes transformation into a postshock state [19] that may cause bump formation.

The bump formation can also be understood by considering that laser pulses induce a large molten layer underneath the ablation layer [20]. A low solidification rate can induce the motion of carbon particles inside the molten layer. After the first pulse, the carbon particles are free to move randomly on the ablated surface and, therefore, agglomerate to form surface clusters. These carbon clusters diffuse into the large molten layer. For succeeding pulses each agglomerate of carbon particles acts as a nucleation site to form bump-like structures [6].

Fig. 2 Raman spectra of the virgin and laser irradiated CR-39 in air for different fluences 0.25 J cm^{-2}, 0.5 J cm^{-2}, 1.5 J cm^{-2}, 2.5 J cm^{-2}, and 3.6 J cm^{-2} after background subtraction
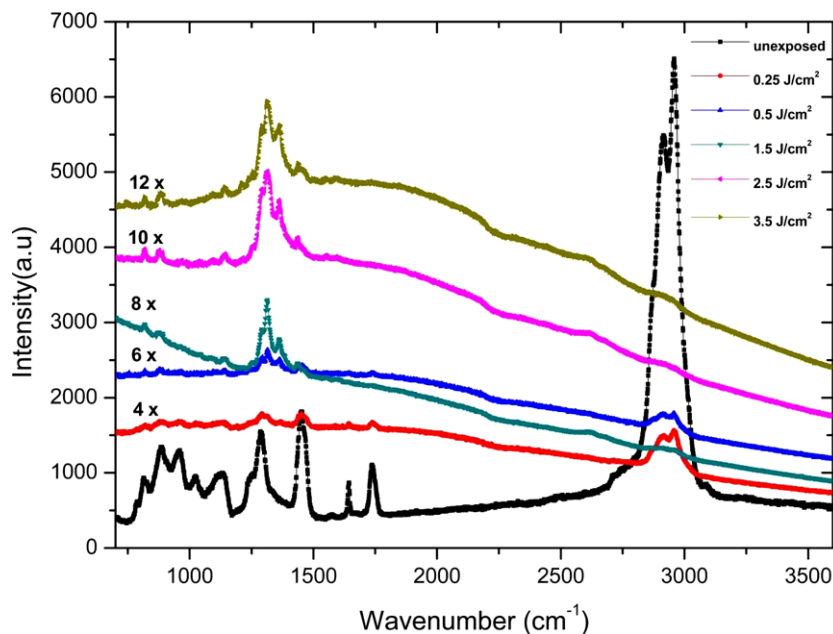
3.2 Raman spectroscopy

Photothermal and photochemical decomposition of the organic polymeric molecules can take place by vibrational or rotational excitation due to absorption of near infrared photons [9]. These processes are responsible for spatially inhomogeneous internal stresses, local volume increase, formation of new bonds, cross linking and bond breaking [21].

In order to have convincing evidence about the structural and chemical changes in the irradiated polymer, Raman spectroscopy has been performed.

Raman spectra of unexposed and exposed CR-39 at different laser fluences are shown in Fig. 2. In a pristine CR-39 target the appearance of peaks at 1287, 1451, 1643, 1737, 2913 and 2958 cm^{-1} confirms its basic monomer structure [4]. The wave numbers around 2913 cm^{-1} and 2958 cm^{-1} are assigned to –CH$_2$– symmetric and asymmetric stretching modes respectively [4]. The spectra show that the density of –CH$_2$– groups reduces significantly after exposure at laser fluences of 0.25 and 0.5 J cm^{-2} and is almost negligible at laser fluences of 1.5, 2.5 and 3.6 J cm^{-2}. This is attributed to the reduction of hydrogen content in the irradiated target for lower laser fluences and its complete absence for higher fluences [22].

At laser fluences of 0.25 and 0.5 J cm^{-2} broadening of these bands is observed with a Raman shift of 4 cm^{-1} in the symmetric stretching mode. A Raman shift at these fluences is attributed to strains developed by radiation induced heating [23]. The observed broadening in the peaks is due to the decrease in phonon lifetime as a result of scattering from radiation-induced defects [24]. In electrical-insulating solids, it is believed that point defects affect the lattice vibrations and cause scattering of phonons due to mass differ-

ences and inter atomic coupling force differences [25] which will shorten the mean free path of the phonons [26].

For higher laser fluence (1.5, 2.5 and 3.6 J cm^{-2}), no peaks are identified for these –CH$_2$– stretching bonds, which is ascribed to complete destruction of these bands.

The two peaks observed at 1737 cm^{-1} and 1643 cm^{-1} correspond to C=O and C=C bands respectively. The intensity of the peaks for these bands is reduced after exposure at a laser fluence of 0.25 J cm^{-2}. For higher laser fluences, ranging from 0.5–3.6 J cm^{-2}, these bands have completely disappeared indicating the destruction of carbonate ester bonds [27], degradation of CR-39 involving carbonyl C=C bond breaking and folding of chains [24].

The band at 1451 cm^{-1} originates from the –C–H– bending mode. For this band, reduced intensity and broadening in the peak is observed for two lower laser fluences i.e. 0.25 and 0.5 J cm^{-2}. This is due to breaking or weakening of –C–H– bonds. When the laser fluence is enhanced to the range of 1.5–3.6 J cm^{-2}, a new peak at 1436 cm^{-1} appears. This new band frequency corresponds to the symmetric CO$_2$– stretching mode. It has already been reported that CO$_2$ molecules are produced in CR-39 when it is irradiated by high-energy ionizing radiation [28–30]. The production of CO$_2$ can be due to the destruction of main chain of CR-39 by irradiation. This is attributed to the break-up of the content of carbonate groups in the vicinity of 1737 cm^{-1}, which corresponds to C=O stretching of –OCOO– groups. This leads to evolution of carbon dioxide gas that is trapped in the polymer material [31]. This trapped CO$_2$ can lead to subsequent crazing and cracking due to accumulated local stresses [30]. These stresses are one of the reasons for explosions which form nano cavities as seen in the surface topography of the irradiated polymer at 1.5 J cm^{-2} (Fig. 1d).

The observed band at 1287 cm^{-1} for the unexposed target corresponds to the C–O stretching mode. For exposed CR-39 some additional peaks are identified. A Raman shift of 4 cm^{-1} for 0.25 J cm^{-2} and 7 cm^{-1} for fluences of 0.5–3.6 J cm^{-2} is observed. At a fluence of 0.5 J cm^{-2} two additional peaks are identified at 1314 and 1363 cm^{-1}. With further increase of the fluence from 1.5 to 3.6 J cm^{-2}, the intensity of these peaks is enhanced. Peak at 1314 cm^{-1} corresponds to the C–O stretching mode and is attributed to oxidation of CR-39 due to its exposure in air. The results indicate that the damage in CR-39 has been produced through radiation-induced oxidation [32]. Laser ablation can break polymer bonds, leaving free radicals that react with dissolved oxygen [33] in CR-39 to form a permanent latent track. These radicals can also recombine to form nanobumps or protrusions, depending on the concentration of oxygen near the ion's path. Identification of additional peaks at higher fluences indicates the enhancement of radiation effects that lead to the formation of more active chemical bonds due to the increase in the degree of cross linking.

The characteristic band at 1363 cm^{-1} can be designated as the well-known disorder D band of hydrogenated amorphous carbon [4] due to the increase in the degree of cross linking. This band is attributed to the formation of a diamond-like carbon (DLC) layer on the irradiated surface of CR-39 which is in agreement with the already reported results on the ion implanted polymide [34] and CR-39 [4].

The relative changes (weakening, broadening, shifting) and appearance of additional peaks observed in the exposed CR-39 suggest that the chemical structure of the polymer is significantly changed after laser irradiation. Thus, Raman spectroscopy reveals that laser irradiation causes bond dissociation, chain scission, free radical formation, cross linking, and formation of new bonds in the polymer.

3.3 Z-scan measurements

The chemical and structural changes will surely lead towards the changes in nonlinear or multiphoton absorption properties of the polymer. The non linear absorption properties of the pristine and irradiated CR-39 have been investigated by a Z-scan measurement technique.

In addition to two-photon absorption, higher order multiphoton absorption can play a substantial role. The theoretical transmission curve given by Bahea [15] has a capacity to be modified, i.e. taking into account three-photon absorption (fifth-order nonlinearities) where the absorption coefficient α can be expressed in terms of the three-photon absorption coefficient α_3 as

$$\alpha = \alpha_0 + \alpha_3 I^2 \tag{1}$$

The amplitude of the electric field $\sqrt{I}$ as a function of z' (coordinate inside the sample) is governed by an equation as follows:

$$\frac{dI}{dz'} = -(\alpha_0 + \alpha_3 I^2)I \tag{2}$$

After lengthy calculations [14], the normalized transmittance $T(z)$, defined as the quotient of transmitted and incident energy, is obtained as

$$T(z) = \sum_{m=0}^{\infty} (-1)^m \frac{P_0(0)^{2m}}{(2m+1)^{3/2} 2m!(1+x^2)^{2m}} \tag{3}$$

Here $P_0(0) = \sqrt{2\alpha_3 L'_{\text{eff}}} I_0(0)$ and $I_0(0)$ is the maximum on-axis intensity at the focus and $x = \frac{z}{z_0}$ that z is the position of the sample measured with respect to the beam waist and z_0 is the Rayleigh length and $L'_{\text{eff}} = \frac{(1-e^{-2\alpha L})}{2\alpha}$ is the effective sample length.

Figure 3(a) shows the experimentally obtained data for unexposed CR-39 and the corresponding fitting curve ob-
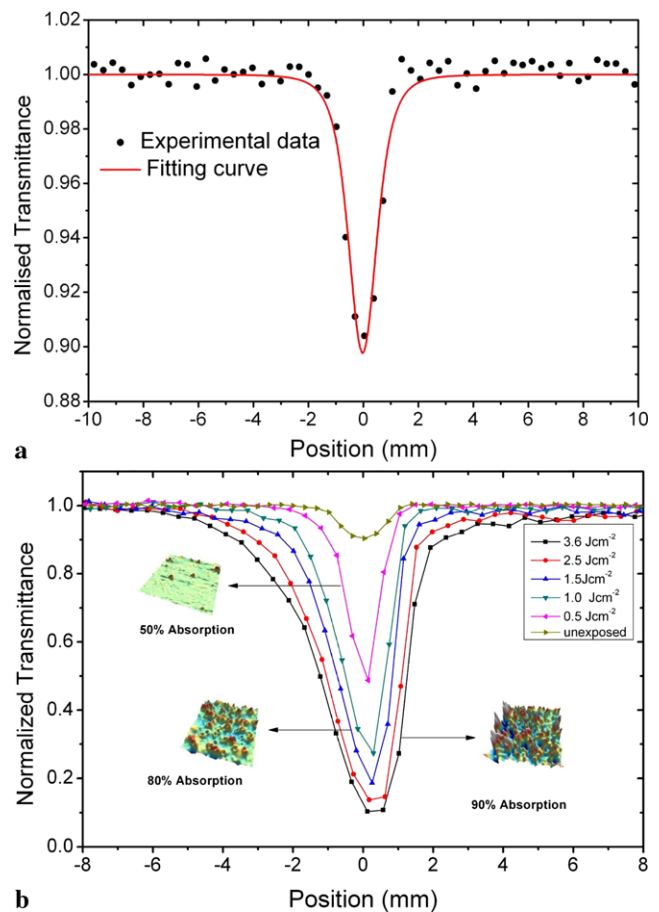
Fig. 3 (**a**) Z-scan measurements for an unexposed CR-39 and the corresponding fitting curves obtained from (3), (**b**) Normalized transmittance/absorption measured by Z-scan technique for ultra short laser irradiated CR-39 at different fluences along with surface micrographs pertaining to the respective fluence
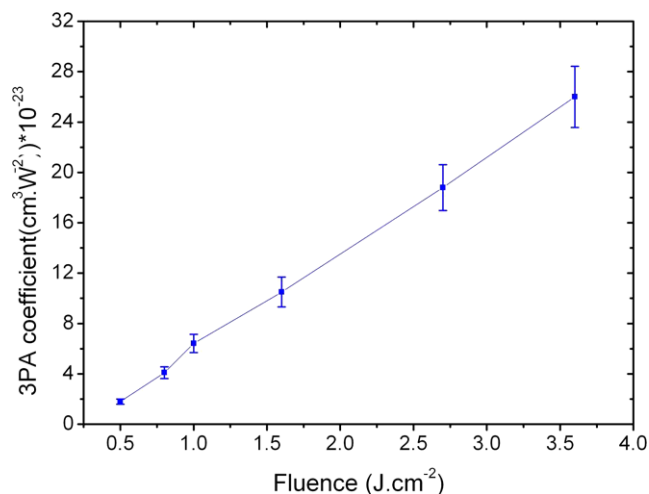
Fig. 4 Three photon absorption coefficient of femtosecond laser irradiated CR-39 for different fluences

tained from equation 3 (three-photon absorption). The three-photon absorption coefficient for this curve is calculated to be $\alpha_3 = 1.0 \pm 0.3 \times 10^{-24}$ cm^3 W^{-2}.

A comparison of experimentally obtained data and the fitting curve from equation 3 clearly indicates the dominance of three-photon absorption in the pristine CR-39. It is an established fact that the first step in the ablation of polymers with 800 nm fs-pulses is the excitation of electrons by multiphoton absorption [35]. A single photon of 800 nm (1.5 eV) is not sufficient to overcome the band gap (3.6 eV indirect and 4.2 eV direct) of CR-39 [10]. This is quite reasonable because the CR-39 band gap is higher than twice the probing photon energy.

Figure 3(b) shows Z-scan measurements for laser irradiated CR-39 at different laser fluences. It is evident that nonlinear absorption of the polymer increases with increasing laser fluence. For the fluence of 0.25 J cm^{-2} no significant change in the nonlinear absorption is observed. Gradual formation of the bumps (Fig. 1(a–e)) and changes in chemical structure (Fig. 2) of CR-39 justifies the increase in nonlinear absorption with the increase in the laser fluence. In addition, the increase in the three-photon absorption maxima (from 1.8×10^{-23} (cm^3 W^{-2}) to 26×10^{-23} (cm^3 W^{-2}) with the laser fluence in Fig. 4 favors a three-photon process. However, it is not necessarily true for the irradiated polymer that the entire absorption is only due to the three-photon process because the polymer undergoes several changes (morphological and compositional) and modifications of the polymerization state as evidenced from AFM images and Raman measurements. These effects could possibly lead to the formation of absorption centers with changes in band gap energies or an energy cut off lower than the three-photon energy and thus to a two-photon absorption. Therefore, the occurrence of both two- and three-photon absorption processes is probable for an irradiated target. However, we have not developed the equation which could explain the co-existence of both the absorption processes.

The optical absorption properties of the polymer are governed by the electronic, vibrational and rotational structure of the molecules. Our AFM and Raman spectra measurements clearly indicate that incident photons have sufficient energy to cause structural modification which can bring about significant changes in the absorption properties of CR-39. Intensive laser fluence causes photochemical decomposition in which electronically excited states undergo internal conversion to the vibrationally excited ground state [36]. Consequently, laser-induced photo-fragmentation changes the binding energies of the neighboring atoms and their coupling to crystal lattice. Mechanism of enhanced density of these vibrationally excited molecules causes a significant enhancement of the multiphoton absorption coefficient of the polymer [37].

The structural destruction of polymer increases the electronic disorder inducing the creation of permitted states in the forbidden (indirect) band or deformation of the valence band [10]. Deformation of valence bands can cause optical modification of the polymer after irradiation because the interactions of light with valence electrons of the material are responsible for optical properties [38]. Lasers can induce structural irregularities or defects in the polymer in the form of stress distributions [39], self-trapped excitons [40], scission of polymer chains [7], formation of free radicals, new bonds and local melting in transparent materials. All these phenomena are responsible for a change in the nonlinear absorption of the irradiated material.

4 Conclusions

Multiphoton absorption properties of CR-39 are strongly influenced by surface modifications, structural and chemical changes induced by an ultra short laser irradiation. Three-photon absorption is found to be dominant process in pristine CR-39. However, the occurrence of both three- and two-photon absorption processes is probable for irradiated CR-39. The enhanced nonlinear absorption with the increase in the laser fluence is the cause of gradual growth of nano bumps, explosions, nano cavities, etc. formed due to stresses. Bond breaking, cross linking and formation of new bonds by energy deposited during the ultra short laser irradiation is also a major cause of significant increase in the non linear absorption of CR-39.

References

1. H.G. Rubahn, *Laser Applications in Surface Science and Technology* (Wiley, New York, 1996)
2. P.C. Kalsi, C. Agarwal, J. Mater. Sci. **43**, 2865 (2008)

3. E. Baradacs, I. Csige, I. Rajta, Radiat. Meas. **43**, 1354 (2008)
4. T. Sharma, S. Aggarwal, A. Sharma, S. Kumar, D. Kanjilal, S.K. Deshpande, P.S. Goyal, J. Appl. Phys. **102**, 063527 (2007)
5. P.C. Kalsi, V.S. Nadkarni, V.K. Manchanda, Radiat. Phys. Chem. **77**, 1002 (2008)
6. H.R. Zangeneh, P. Parvin, Z. Zamanipour, B. Jaleh, S. Jelvani, M. Taheri, Radiat. Eff. Defects Solids **163**, 863 (2008)
7. S. Bashir, M.S. Rafique, F. Ul-Haq, Laser Part. Beams **25**, 181 (2007)
8. F. Abu-Jarad, S.M.A. Durrani, M.A. Islam, Nucl. Instrum. Methods Phys. Res. B **74**, 419 (1993)
9. A.A. Serafetinides, M. Makropoulou, E. Fabrikesi, E. Spyratou, C. Bacharis, R.R. Thomson, A.K. Kar, Appl. Phys. A: Mater. Sci. Process. **93**, 111 (2008)
10. M.F. Zaki, J. Phys. D, Appl. Phys. **41**, 75404 (2008)
11. T. Yamauchi, Y. Mori, K. Oda, N. Yasuda, H. Kitamura, B. Rémi, Jpn. J. Appl. Phys. **47**, 3606 (2008). Part 1: Regular Papers and Short Notes and Review Papers
12. T. Sharma, S. Aggarwal, A. Sharma, S. Kumar, V.K. Mittal, P.C. Kalsi, V.K. Manchanda, Radiat. Eff. Defects Solids **163**, 173 (2008)
13. C. Gan, Y. Zhang, S.W. Liu, Y. Wang, M. Xiao, Opt. Mater. **30**, 1440 (2008)
14. A. Ajami, M.S. Rafique, N. Pucher, S. Bashir, W. Husinsky, R. Liska, R. Inführ, H. Lichtenegger, J. Stampfl, St. Lüftenegger, in *Z-scan Measurements of Two-photon Absorption for Ultrashort Laser Radiation.* Proc. SPIE, vol. 7027 (SPIE, Bellingham, 2008)
15. M. Sheik-Bahae, A.A. Said, T.-H. Wei, D.J. Hagan, E.W. Van Stryland, IEEE J. Quantum Electron. **26**, 760 (1990)
16. M. Schmidt, R. Kusche, B. von Issendorff, H. Haberland, Nature **393**, 238–240 (1998)
17. A. Vogel, V. Venugopalan, Chem. Rev. **103**, 577 (2003)
18. V. Koubassov, J.F. Laprise, F. Théberge, E. Förster, R. Sauerbrey, B. Müller, U. Glatzel, S.L. Chin, Appl. Phys. A, Mater. Sci. Process. **79**, 499 (2004)
19. H. Ma, G. Guo, J. Yang, Y. Guo, N. Ma, Nucl. Instrum. Methods Phys. Res., Sect. B: Beam Interact. Mater. Atoms **264**, 61 (2007)
20. P.E. Dyer, S.D. Jenkins, J. Sidhu, Appl. Phys. Lett. **49**, 453 (1986)
21. J. Vanderschueren, G. Yianakopoulos, J. Niezette, C. Chatry, J. Gasiot, J. Appl. Polym. Sci. **44**, 1027 (1992)
22. J.S. Chen, S.P. Lau, Z. Sun, B.K. Tay, G.Q. Yu, F.Y. Zhu, D.Z. Zhu, H.J. Xu, Surf. Coat. Technol. **138**, 33 (2001)
23. R.J. Young, W.Y. Yeh, Polymer **35**, 3844 (1994)
24. B. Mallick, R.C. Behera, T.N. Tiwari, S. Panigrahi, S.K. Samal, Radiat. Eff. Defects Solids **163**, 161 (2008)
25. X. Shi, L. Chen, J. Yang, G.P. Meisner, Appl. Phys. Lett. **84**, 2301 (2004)
26. C.L. Wan, W. Pan, Q. Xu, Y.X. Qin, J.D. Wang, Z.X. Qu, M.H. Fang, Phys. Rev. B, Condens. Matter Mater. Phys. **74** (2006)
27. Y. Mori, T. Ikeda, T. Yamauchi, A. Sakamoto, H. Chikada, Y. Honda, K. Oda, Radiat. Meas. (2009)
28. C.S. Chong, I. Ishak, R.H. Mahat, Y.M. Amin, Radiat. Meas. **28**, 119 (1997)
29. A.F. Saad, S.T. Atwa, R. Yokota, M. Fujii, Radiat. Meas. **40**, 780 (2005)
30. M.A. Malek, C.S. Chong, Radiat. Meas. **35**, X203 (2002)
31. M.A. Malek, C.S. Chong, Vibr. Spectrosc. **24**, 181 (2000)
32. T. Yamauchi, Radiat. Meas. **36**, 73 (2003)
33. T. Yamauchi, S. Takada, H. Ichijo, K. Oda, Radiat. Meas. **34**, X69 (2001)
34. J.M. Costantini, J.P. Salvetat, F. Couvreur, S. Bouffard, Nucl. Instrum. Methods Phys. Res., Sect. B: Beam Interact. Mater. Atoms **234**, 458 (2005)
35. C. Wochnowski, Y. Hanada, Y. Cheng, S. Metev, F. Vollertsen, K. Sugioka, K. Midorikawa, J. Appl. Polym. Sci. **100**, 1229 (2006)
36. B. Jaleh, P. Parvin, K. Mirabaszadeh, M. Katouzi, Radiat. Meas. **38**, 173 (2004)
37. W.W. Duley, *UV Lasers Effects and Applications in Material Science* (Cambridge University Press, Cambridge, 1996)
38. R.E. Hummel, *Electronic Properties of Materials* (Springer, Berlin, 1993)
39. A.A. Serafetinides, M.I. Makropoulou, C.D. Skordoulis, A.K. Kar, Appl. Surf. Sci. **180**, 42 (2001)
40. C.W. Ponader, J.F. Schroeder, A.M. Streltsov, J. Appl. Phys. **103**, 063516 (2008)